XMM#Newton Observations of Red AGNs

The Astrophysical Journal, 634:183–192, 2005 November 20

XMM-NEWTON OBSERVATIONS OF RED AGNs

B. J. Wilkes,[1] K. A. Pounds,[2] G. D. Schmidt,[3] P. S. Smith,[3] R. M. Cutri,[4] H. Ghosh,[5] B. Nelson,[4] and D. C. Hines[6]

Received 2004 November 30; accepted 2005 June 26

ABSTRACT

XMM-Newton spectra of five red 2MASS active galactic nuclei (AGNs), selected from a sample observed by *Chandra* to be relatively X-ray bright and to cover a range of hardness ratios, confirm the presence of substantial absorbing material in three sources with optical classifications ranging from type 1 to type 2. A flat (hard) power-law continuum is observed in the other two. The combination of X-ray absorption and broad optical emission lines suggests either a small (nuclear) absorber or a favored viewing angle so as to cover the X-ray source but not the broad emission-line region (BELR). A soft excess is detected in all three type 1 sources. We speculate that this may arise in an extended region of ionized gas, perhaps linked to the polarized (scattered) optical light present in these sources. The spectral complexity revealed by *XMM-Newton* emphasizes the limitations of the low-S/N *Chandra* data. The new results strengthen our earlier conclusions that the observed X-ray continua of red AGNs are unusually hard at energies $\gtrsim$2 keV. Their observed spectra are consistent with contributing significantly to the missing hard or absorbed population of the cosmic X-ray background (CXRB), although their intrinsic power-law slopes are typical of broad-line (type 1) AGNs ($\Gamma \sim 1.7$–1.9). This suggests that the missing X-ray–absorbed CXRB population may include type 1 AGNs or QSOs in addition to the type 2 AGNs generally assumed.

Subject headings: galaxies: active — galaxies: nuclei — X-rays: galaxies

Online material: color figures

1. INTRODUCTION

The Two Micron All Sky Survey (2MASS) has revealed a large number of highly reddened active galaxies (AGNs) not previously found in optical/UV color-selected surveys (Cutri et al. 2002; Francis et al. 2004). Their typically high optical polarization (Smith et al. 2002, 2003) suggests substantial obscuration around the nuclear energy source. *Chandra* observations show weak, hard X-ray emission compared with normal, broad-line, low-redshift AGNs, suggesting that these mostly broad-line AGNs are absorbed. Evidence for a significant population of X-ray–absorbed, broad-line AGNs in both individual sources and samples is growing (Silverman et al. 2005; Perola et al. 2004). Broad absorption line (BAL) QSOs are another well-defined subset with this property (Green et al. 2001). Notably, BAL QSOs also have high optical polarization levels. As X-ray–absorbed AGNs, these sources may contribute to the X-ray–absorbed population predicted by modeling of the cosmic X-ray background (CXRB; Gilli et al. 2001; Comastri et al. 1995).

The realization that obscuration plays a critical role in the classification of AGNs inspired a fundamental change in our understanding of the phenomenon. Not only does the "unified scheme" (Antonucci 1993) provide a basis for new observations and theoretical models, but it also implies that many AGNs may be missed in UV-excess surveys (e.g., Masci et al. 1999). Ideas of what constitutes an AGN continue to expand as X-ray and radio surveys find luminous, unresolved sources that show no signs of activity at other wavelengths (e.g., Elvis et al. 1981; Bauer et al. 2004), implying that the overall number density has been significantly underestimated. Ramifications include revisions of the fraction and types of galaxies that harbor an active nucleus, the energy density of ionizing radiation in the young universe, the nature of the X-ray and far-IR backgrounds, and the importance of accretion power in the universe as a whole.

Although the *Infrared Astronomical Satellite* (*IRAS*) provided the first significant sample of extragalactic objects in which the bulk of the luminosity emerges as reprocessed radiation in the IR (Soifer et al. 1984), its sensitivity was sufficient to catalog only the most nearby and/or luminous AGNs. 2MASS has yielded a much deeper catalog of near-IR–selected AGNs (Cutri et al. 2002) by selecting sources with $J - K_s > 2$ from the high Galactic latitude 2MASS Point Source Catalog. Spectroscopic follow-up of red candidates reveals that $\sim$75% are previously unidentified emission-line AGNs, with $\sim$80% of these showing broad optical emission lines (type 1: Seyfert type 1 and QSO), and the remainder are narrow-line objects (type 2: Seyfert type 2, QSO type 2, and low-ionization nuclear emission-line region [LINER]; Cutri et al. 2002). They span a redshift range $0.1 < z < 2.3$ with median $z \sim 0.25$. The inferred surface density is $\sim$0.5 deg^{-2} brighter than $K_s < 14.5$, higher than that of optically selected AGNs at the same IR magnitudes, indicating that 2MASS will reveal >25,000 such objects over the sky. The objects also have unusually high optical polarization levels, with $\sim$10% showing $P > 3\%$, indicating a significant contribution from scattered light (Smith et al. 2002, 2003).

In a near-infrared flux-limited survey for AGNs, largely unbiased by color selection, Francis et al. (2004) found that the fraction of all galaxies harboring AGNs increases with increasing $J - K_s$ color. They could not place stringent limits on the total fraction of dust-reddened AGNs at low redshift, however, because the optical colors are dominated by host-galaxy light and because of poor statistics for the reddest and optically faintest sources. Obscuration by dust may very well account for the lower contrast of the nuclear emission at optical wavelengths while

[1] Harvard-Smithsonian Center for Astrophysics, 60 Garden Street, Cambridge, MA 02138.
[2] Department of Physics and Astronomy, University of Leicester, University Road, Leicester LE1 7RH, UK.
[3] Steward Observatory, University of Arizona, 933 North Cherry Avenue, Tucson, AZ 85721.
[4] Infrared Processing and Analysis Center, California Institute of Technology, MS 100-22, Pasadena, CA 91125.
[5] Department of Astronomy, Ohio State University, 4055 MacPherson Laboratory, 180 West 18th Avenue, Columbus, OH 43210-1173.
[6] Space Science Institute, 4750 Walnut Street, Suite 205, Boulder, CO 80301.

TABLE 1
XMM-Newton Observation Details

	pn Camera			MOS Cameras		
2MASS J	Filter	Exposure (s)	Counts	Filter	Exposure (s)	Counts
09184860+2117170	Thin	5439	288 ± 60	Thin	16098	241 ± 32
10514425+3539306	Thin	3044	1126 ± 61	Medium	10645	1490 ± 43
13000534+1632149	Medium	1184	284 ± 59	Medium	5355	396 ± 32
14025120+2631175	Medium	1699	1648 ± 51	Medium	4937	1136 ± 44
23444958+1221432	Thin	4444	844 ± 73	Thin	13164	790 ± 38

leaving the near-infrared nuclear colors largely unaffected. A better estimate of the fraction of extinguished AGNs comes from Glikman et al. (2004), who examined a sample of Faint Images of the Radio Sky at Twenty cm (FIRST) radio sources with 2MASS near-infrared detections but without optical counterparts. They concluded that this population accounts for approximately 20% of all QSOs.

The *Röntgensatellit* (*ROSAT*) found that, while known AGNs dominate the soft (0.1–2.0 keV) CXRB (Lehmann et al. 2000), an additional population of heavily absorbed AGNs would be required to account for the harder high-energy spectrum (Comastri et al. 1995). To match both the CXRB spectrum and the observed hard X-ray number counts of other pre-*Chandra* surveys (e.g., *BeppoSAX*; Fiore et al. 2001), the X-ray–absorbed AGN population is estimated to outnumber unabsorbed AGNs by ~4:1 and perhaps to increase with z (Gilli et al. 2001; Comastri et al. 2001). Although the local ratio of type 2 to type 1 AGNs appears to be ~2–4 (Maiolino & Rieke 1995; Huchra & Burg 1992), a large, thus far undiscovered population of X-ray–absorbed AGNs at higher z was required by these models.

XMM-Newton and *Chandra* are finding objects in sufficient numbers to explain 85%–90% of the CXRB at energies $\lesssim$5 keV (Bauer et al. 2004; Worsley et al. 2004). While these include a significant number of hard-spectrum sources, most are at low redshift, contrary to the expectations of the models (Gilli et al. 2001). Wider area surveys, which are more able to characterize the absorbed population, are beginning to find higher redshift absorbed sources (Fiore et al. 2003; Treister et al. 2005), approaching the model predictions. The hard X-ray sources correspond to both optically faint objects and bright, nearby elliptical galaxies, as well as more traditional broad-line or narrow-line AGNs (Silverman et al. 2005). They frequently have red continua ($1.5 < J - K_s < 2.5$) that, combined with their optical colors, are consistent with the moderate amounts of gas and dust absorption required to match the CXRB at energies <10 keV (Compton-thin; equivalent neutral hydrogen column density $N_{\rm H} \leq 10^{22}$–10^{23} cm^{-2}). Thus, evidence is mounting that absorbed AGNs are indeed important contributors to the CXRB, although in some cases their nuclei are only visible at X-ray wavelengths. Given the high surface density and similarities of the new population of 2MASS AGNs to the absorbed AGNs being found in the X-ray surveys, a census of the X-ray properties of the 2MASS AGNs will aid our understanding of them and show whether this previously missed population contributes significantly to the CXRB.

We have surveyed a well-defined, color-selected subset of 44 2MASS AGNs (Wilkes et al. 2002) using the Advanced CCD Imaging Spectrometer array (ACIS; Nousek et al. 1998) on *Chandra*. The subset was selected to have $B - K_s > 4.3$ and $K_s < 13.8$, including the brightest and reddest objects but covering sufficient parameter space to be representative of the new population: $0 < z < 0.4$ and $0\% < P < 9.3\%$ (Smith et al. 2000) and a full range of optical classes. A comparison of the K_s band to 1 keV flux density ratios ($F_{\rm X}/F_K$, the latter computed assuming a *normal* AGN X-ray spectrum; $N_{\rm H} = 3 \times 10^{20}$ cm^{-2}, $\Gamma = 2$) with those of low-redshift, broad-line AGNs (see Fig. 1 in Wilkes et al. 2002) demonstrates the general weakness of X-ray emission from the 2MASS QSOs, placing them in the range measured for BAL QSOs and Seyfert 2 galaxies. The reddest AGNs in the sample ($J - K_s > 2.5$) are the weakest X-ray sources, suggesting that absorption by related dust and gas affects the emission in the IR and X-ray bands, respectively.

The *Chandra* observations, aimed at detecting the AGNs, generally have too low signal-to-noise ratios (S/Ns) to provide constraints on the X-ray spectra and absorption beyond those of hardness ratios or simple power-law fits. A normal AGN X-ray spectrum with little absorption yields a *Chandra* hardness ratio [HR $= (H - S)/(S + H)$, where S and H are the net counts in the energy bands 0.3–2.5 and 2.5–8 keV, respectively] of HR $= -0.7$ (ACIS-S, Cycle 4). The 2MASS sample covers the range $-0.6 <$ HR < 0.6, consistent with absorbing columns of $N_{\rm H} = 10^{21}$–10^{23} cm^{-2} for most sources. Spectral fits for those with higher counts reinforce this conclusion (B. J. Wilkes et al. 2005, in preparation). Two 2MASS AGNs are consistent with no absorption above the Galactic column (HR < -0.5). Contrary to a simple absorption scenario in which a single screen of gas and dust obscures all continuum-emitting regions, there is no correlation between HR and $J - K_s$; that is, while they are X-ray–weak, the reddest objects are not necessarily those with the hardest X-ray emission. However, AGN X-ray spectra often contain a number of components that modify the power-law continuum emission believed to originate in the central AGN. In addition to cold absorbing material, these may include partial covering of the source, an ionized absorber, soft excess emission, and scattering or reflection by neutral and/or ionized material. Such complexity can strongly affect the interpretation of a simple hardness ratio determined from the low-S/N *Chandra* spectra.

Correction of the X-ray flux for absorption on the basis of the hardness ratios moves only about half of the 2MASS sample into the X-ray–faint region occupied by the Elvis et al. (1994) broad-line AGNs in $F_{\rm X}/F_K$ (B. J. Wilkes et al. 2005, in preparation) or even the X-ray weaker, optically selected sample of Laor et al. (1997). Possible explanations for this X-ray weakness include a high K_s flux due to either increased hot dust emission or the inclusion of extended, host galaxy emission in these mostly low-redshift sources, intrinsically faint and hard X-ray emission, or complex X-ray spectra that result in our underestimating their intrinsic X-ray flux.

With the aim of removing these ambiguities for at least a subset of the *Chandra* sample of 2MASS AGNs, we recently

TABLE 2

Chandra X-Ray and Optical Parameters

2M[a]	Redshift	Γ[b]	$N_{\rm H\ int}$ (10^{21} cm^{-2})	HR	$J-K_s$	$B-R$ (DSS)	Class[c]	P[d] (%)
0918.....	0.149	1.9 ± 0.5	2 ± 2	-0.6 ± 0.1	2.23 ± 0.04	2.1	1.5	10.01 ± 0.07
1051.....	0.158	1.6 ± 0.2	5.6 ± 1.4	-0.2 ± 0.1	2.08 ± 0.07	2.6	1.9	0.54 ± 0.29
1300.....	0.080	1.5 ± 0.8	18 ± 10	0.2 ± 0.1	2.17 ± 0.05	3.1	2.0	9.50 ± 0.07
1402.....	0.187	2.0 ± 0.4	0.1 ± 1.3	-0.6 ± 0.1	2.08 ± 0.05	0.6	1.0	0.21 ± 0.21
2344.....	0.199	2.0 ± 0.4	4 ± 2	-0.4 ± 0.1	2.00 ± 0.06	1.3	1.0	1.01 ± 0.24

[a] See § 4 for a discussion of abbreviated source names.
[b] Power-law plus absorption fit over the 0.5–8 keV band.
[c] The optical class ranges from 1.0 to 2.0 on the basis of the ratio of narrow to broad emission lines.
[d] Optical percent polarization (Smith et al. 2002, 2003).

obtained *XMM-Newton* spectra of five representative sources (Table 1). Improved X-ray spectra will clarify the relationship to other AGN properties such as optical and IR color, optical polarization, and the X-ray–to–IR ratio. Understanding the individual sources is a key to determining the relation of these new, red, X-ray–absorbed, broad-line AGNs to the remainder of the AGN population. Throughout this paper, we assume $H_0 = 70$ km s^{-1} Mpc^{-1}, $\Omega_\Lambda = 0.7$, and $\Omega_M = 0.3$.

2. OBSERVATIONS

Details of the *XMM-Newton* observations of the 2MASS sources are given in Table 1. X-ray data were available throughout each observation from the EPIC pn (Strüder et al. 2001) and MOS (Turner et al. 2001) cameras, providing moderate resolution spectra (35 eV at Al-K [1.5 keV] and 61 eV at Mn-K [5.9 keV]) over the energy band ~0.3–10 keV.

The X-ray data were first screened with the *XMM-Newton* Science Analysis System (SAS) version 5.4 software and events corresponding to patterns 0–4 (single- and double-pixel events) were selected for the pn data and patterns 0–12 for MOS1 and MOS2, the latter then being combined. A low-energy cutoff of 300 eV was applied to all X-ray data, and known hot or bad pixels were removed. Source counts were obtained from a circular region of 45″ radius centered on the target source, with the background being taken from a similar region offset from, but close to, the source. Unfortunately, the background was high during parts of each observation, and these data have been excluded from the subsequent spectral analysis, using the recommended cutoff background rates of 1 s^{-1} (pn camera) and 0.35 s^{-1} (MOS camera). The resulting exposures and source counts are listed in Table 1. The integrated data set for each source was then available for spectral analysis. Individual EPIC spectra were binned to a minimum of 20 counts per bin to facilitate use of the χ^2 minimization technique in spectral fitting. Spectral fitting was based on the XSPEC package (Arnaud 1996), and all fits included absorption due to the relevant line-of-sight Galactic column. Errors are quoted at the 90% confidence level ($\Delta\chi^2 = 2.7$ for one interesting parameter).

3. X-RAY SPECTRAL ANALYSIS

The optical and *Chandra* X-ray properties of the five AGNs are listed in Table 2 and repeated here as we describe the X-ray spectral fitting of the *XMM-Newton* data. Note that the *Chandra* fits were made over the 0.3–8 keV band, with a power law plus cold absorption (using the CIAO software; Fruscione & Siemiginowska 2000). In assessing the *XMM-Newton* spectra, we first fitted a power law to the energies $\gtrsim$2 keV. This is the conventional approach in analyzing AGN X-ray spectra, generally to minimize the effects of absorption. More particularly, in this study that approach allows a direct comparison of individual source spectra with the CXRB, which has the form of a power law of photon index $\Gamma = 1.4 \pm 0.1$ above ~2 keV. The pn and MOS data are fitted simultaneously in each case, with only the power-law index and normalization untied.

3.1. *2MASS J09184860+2117170*

In the optical this source shows an intermediate (1.5) spectral classification and lies at a redshift of $z = 0.149$. The Galactic column is $N_{\rm H} = 4.1 \times 10^{20}$ cm^{-2}. It is a highly reddened object in the *Chandra* sample, with $J - K_s = 2.23$, but the *Chandra*

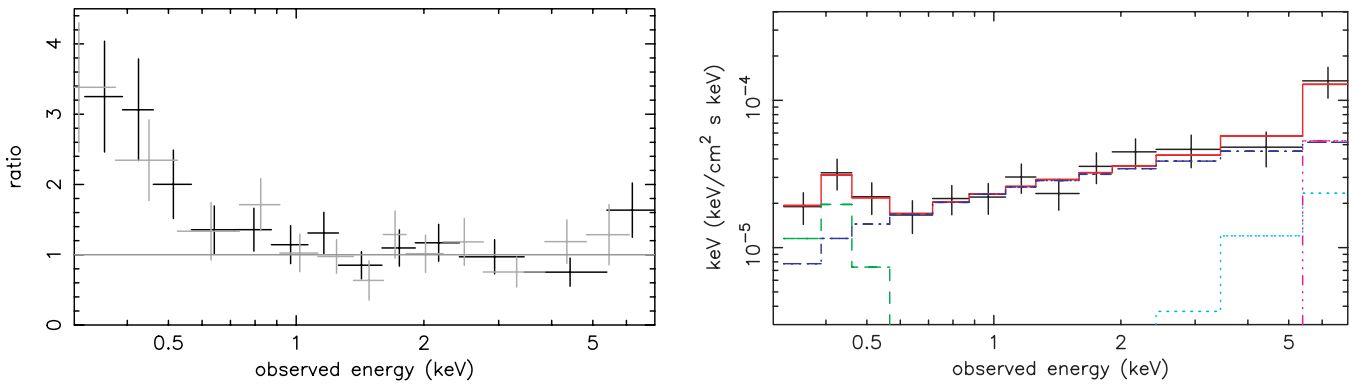

FIG. 1.—2MASS J09184860+2117170. *Left*: Ratio of pn (*black*) and MOS (*gray*) EPIC spectral data to a hard power-law fit above 2 keV, revealing a soft excess and evidence for reflection in the highest energy channels. *Right*: Unfolded spectrum (*black*), illustrating the best-fit spectrum (*red*), with a power-law (*dark blue*) plus reflection component (*light blue*), the Fe Kα line component (*magenta*), and a soft emission component (*green*). Only pn camera data are shown, for clarity. [*See the electronic edition of the Journal for a color version of the left panel of this figure.*]

TABLE 3
XMM-Newton X-Ray Spectral Parameters (pn Camera)

2M[a]	Γ(2–10)	Γ(0.3–10, pn)	N_H (10^{21} cm^{-2})	Line Energy (keV)	Line Flux[b]	χ^2/dof
0918.....	1.26 ± 0.39	1.65 ± 0.33[c]	<1.1[d]	0.44 ± 0.13	4×10^{-5}	13/20
1051.....	1.67 ± 0.11	1.79 ± 0.08	7.2 ± 0.7	...	...	103/115
1300.....	1.16 ± 0.16	1.74 ± 0.26	29 ± 5	6.2 ± 0.35	1.3×10^{-5}	11/24
1402.....	1.53 ± 0.16	1.54 ± 0.07	<0.4[d]	0.44 ± 0.10	4×10^{-4}	110/102
2344.....	1.70 ± 0.16	1.86 ± 0.12	6.5 ± 2.6	0.64 ± 0.05	1×10^{-4}	65/69

[a] See § 4 for a discussion of abbreviated source names.
[b] Units are photon cm^{-2} s^{-1}.
[c] The best-fit model includes a cold reflection component: $R \sim 5$ and EW(Fe Kα) ~ 0.5 keV at 6.4 keV.
[d] 90% upper limit. When absorption at this level is included, the best-fit power law becomes $\Gamma = 1.8$ for 2M 0918 and $\Gamma = 1.64$ for 2M 1402.

data are soft (HR $= -0.6$), and a simple broadband power-law fit yields a power-law index close to that for a normal, unabsorbed Seyfert 1 galaxy (Table 2). Thus, if absorption is responsible for the red color, X-ray spectral complexity must be present, causing the X-ray absorption to be underestimated in a simple power-law fit.

XMM-Newton observed this source to be a factor of ∼4–5 fainter than during the *Chandra* observation. Fitting the pn and MOS data to a power law above 2 keV yielded flat but poorly constrained spectral indexes of $\Gamma = 1.26 \pm 0.39$ (pn) and 1.21 ± 0.42 (MOS). Extrapolating this power law to 0.3 keV was clearly a poor fit ($\chi^2 = 59$ for 25 degrees of freedom [dof]) with a soft excess and also some upward curvature in the highest energy channels (Fig. 1, *left*). Since the latter was suggestive of reflection, a further power-law fit was made, now including the data down to 1 keV (to tighten the constraints) and adding a cold reflection component modeled in XSPEC by `pexrav` (Magdziarz & Zdziarski 1995). The best fit had a high reflection component, with $R \sim 6$. The power-law index increased by ∼0.3 in this fit, but the soft excess remained. Adding a blackbody then provided an acceptable fit over the whole 0.3–8 keV energy band. Interestingly, a Gaussian emission "line" matched the soft excess better, and this is included in the best-fit model ($\chi^2 = 13$ for 20 dof) reproduced in Figure 1 (*right*). The parameters of the best-fit model are an underlying power-law index $\Gamma = 1.65 \pm 0.33$ (pn) and 1.56 ± 0.38 (MOS), with cold reflection [$R \sim 5$, EW(Fe Kα) ~ 0.5 keV] and a Gaussian emission line at 0.44 ± 0.13 keV, with line width $\sigma \sim 75$ eV and flux $\sim 4 \times 10^{-5}$ photons cm^{-2} s^{-1} (Table 3). This "line" is a rough approximation to the blend of line emission expected from ionized gas. More detailed modeling of this feature, unwarranted in the current low-S/N data, would require an accounting for the uncertain energy calibration below $E \sim 0.5$ keV.[7]

We determine an upper limit on the X-ray column density, $N_H \lesssim 1.1 \times 10^{21}$ cm^{-2} (90% confidence). Including absorption at this level in the spectral fit steepens the deduced power law to $\Gamma \sim 1.8$, well within the normal range.

The observed energy fluxes (pn camera; Table 4) were 4.1×10^{-14} ergs cm^{-2} s^{-1} (0.3–1 keV), 3.2×10^{-14} ergs cm^{-2} s^{-1} (1–2 keV), and 1.9×10^{-13} ergs cm^{-2} s^{-1} (2–10 keV). The overall 0.3–10 keV luminosity was 1.4×10^{43} ergs s^{-1}, with 6×10^{41} ergs s^{-1} in the Gaussian soft X-ray emission component.

3.2. *2MASS J10514425+3539306*

At a redshift of $z = 0.158$, this source has been optically classified as a type 1.9 QSO (Smith et al. 2003). The Galactic column is $N_H = 1.9 \times 10^{20}$ cm^{-2}. Although less strongly reddened than 2MASS J09184860+2117170, it had a harder HR $= -0.2$ in the *Chandra* observation. The *Chandra* data had sufficient counts to determine a power-law fit of $\Gamma = 1.6 \pm 0.2$ attenuated by a column of $N_H = (5.6 \pm 1.4) \times 10^{21}$ cm^{-2}.

The *XMM-Newton* data confirmed and further constrained the *Chandra* spectral fit. A power law for energies ≳2 keV yielded photon indexes $\Gamma = 1.67 \pm 0.11$ (pn) and 1.51 ± 0.11 (MOS). When extrapolated to a lower energy, strong attenuation is evident (Fig. 2, *left*). Refitting the data over the 0.3–9 keV band with a power law plus absorber (modeled by the photoionized absorber model, `absori` in XSPEC) produced an excellent

[7] As discussed in *XMM-Newton* document XMM-SOC-CAL-TN-0018 by Kirsch (2004).

TABLE 4
XMM-Newton X-Ray Fluxes and Luminosities

2M[a]	Flux(0.3–1 keV)[b] (10^{-13})	Flux(1–2 keV)[b] (10^{-13})	Flux(2–10 keV)[b] (10^{-12})	L(0.3–10 keV)[c] (10^{44})	L_{SX}[d] (10^{42})
0918.....	0.41	0.32	0.19	0.14	0.6
1051.....	0.5	4	2.0	2.3	...
1300.....	0.14	1.45	2.35	0.68	...
1402.....	7.5	4.7	1.9	2.6	16
2344.....	0.9	1.4	0.51	0.79	2.9

[a] See § 4 for a discussion of abbreviated source names.
[b] Units of flux are ergs cm^{-2} s^{-1}.
[c] Absorption-corrected luminosity in units of ergs s^{-1}.
[d] Absorption-corrected luminosity of the soft excess component in units of ergs s^{-1}.

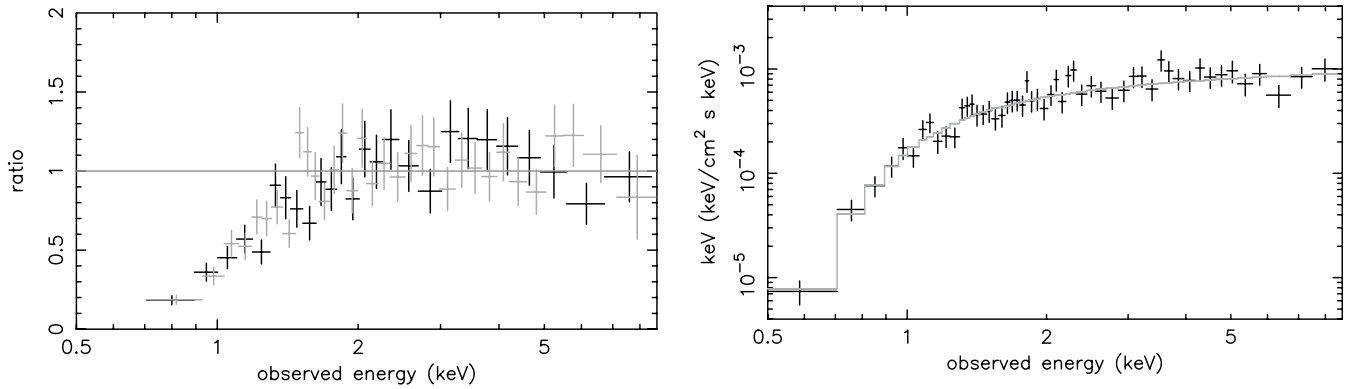

FIG. 2.—2MASS J10514425+3539306. *Left*: Ratio of pn (*black*) and MOS (*gray*) EPIC spectral data to a simple power-law fit above 2 keV, showing a strong low-energy cutoff. *Right*: Unfolded spectrum (*black*), illustrating the best-fit attenuated power-law model (*gray*). Only pn camera data are shown, for clarity. [*See the electronic edition of the Journal for a color version of the left panel of this figure.*]

fit ($\chi^2 = 103$ for 115 dof), with an absorbing column (solar abundances) of cold matter ($\xi \leq 0.7$) of $N_{\rm H} = (7.2 \pm 0.7) \times 10^{21}$ cm^{-2}. The power-law index steepened in this broadband fit (reproduced in Fig. 2, *right*) to $\Gamma = 1.79 \pm 0.08$ (pn) and 1.70 ± 0.08 (MOS).

The observed fluxes (pn camera; Table 4) were 5×10^{-14} ergs cm^{-2} s^{-1} (0.3–1 keV), 4×10^{-13} ergs cm^{-2} s^{-1} (1–2 keV), and 2.0×10^{-12} ergs cm^{-2} s^{-1} (2–10 keV). The observed 0.3–10 keV luminosity was 1.5×10^{44} ergs s^{-1} and was 2.3×10^{44} ergs s^{-1} with the absorbing column removed. Such a high luminosity supports the identification of 2MASS J10514425+3539306 as a QSO rather than a LINER or starburst galaxy. In addition, detailed comparison of the X-ray fluxes shows that the source had brightened by a factor of $\sim$1.5–2 between the *Chandra* and *XMM-Newton* observations, which is larger than the current uncertainties in cross-calibration.

3.3. *2MASS J13000534+1632149*

This object is optically classified as a type 2 QSO (Schmidt et al. 2002; Smith et al. 2003), updated from the 1.x classification in Smith et al. (2002), which was based on a low-S/N discovery spectrum. It lies at a redshift of $z = 0.080$, and the Galactic column is $N_{\rm H} = 2.0 \times 10^{20}$ cm^{-2}. *Chandra* found this source to have the hardest spectrum of our subset, with HR = 0.2 (Wilkes et al. 2002), $\Gamma = 1.5$, and $N_{\rm H} \sim 1.8 \times 10^{22}$ cm^{-2} (Table 2). The *XMM-Newton* observation found an X-ray flux level essentially unchanged from the *Chandra* value ($\leq$20% change based on the predicted vs. observed *XMM-Newton* count rates).

A power-law fit for energies $\gtrsim$2 keV yielded very flat (hard) photon indexes of $\Gamma = 1.16 \pm 0.16$ (pn) and 1.1 ± 0.2 (MOS), with an extrapolation to lower energies showing a cutoff similar to that in 2MASS J10514425+3539306 (Fig. 3, *left*). Adding `absori` to model the attenuation, the best-fit power law steepened to $\Gamma = 1.67 \pm 0.20$ (pn) and 1.65 ± 0.21 (MOS), with a large absorbing column (solar abundances) of $N_{\rm H} = (2.9 \pm 0.5) \times 10^{22}$ cm^{-2}. The ionization parameter ($\xi = L/nr^2$) was $\xi = 4.1 \pm 1.7$, indicating that the absorbing material is, at most, only weakly ionized.

Although the absorbed power-law fit was statistically very good ($\chi^2 = 20$ for 28 dof), the residuals showed an excess near 6 keV. Adding a narrow Gaussian line to the model further improved the fit to $\chi^2 = 11$ for 24 dof, with a line energy (AGN rest frame) of 6.20 ± 0.35 keV and EW $\sim$ 250 eV. This addition to the model resulted in a further steepening of the power-law index by $\sim$0.1. Figure 3 (*right*) illustrates the best-fit power-law spectrum.

The observed fluxes (pn camera; Table 4) were 1.4×10^{-14} ergs cm^{-2} s^{-1} (0.3–1 keV), 1.45×10^{-13} ergs cm^{-2} s^{-1} (1–2 keV), and 2.35×10^{-12} ergs cm^{-2} s^{-1} (2–10 keV). The observed 0.3–10 keV luminosity was 3.7×10^{43} ergs s^{-1} and was 6.8×10^{43} ergs s^{-1} with the absorbing column removed.

3.4. *2MASS J14025120+2631175*

The final two objects in our sample are optically classified as type 1 QSOs. 2MASS J14025120+2631175 is at a redshift of $z = 0.187$, and the Galactic column is $N_{\rm H} = 1.4 \times 10^{20}$ cm^{-2}.

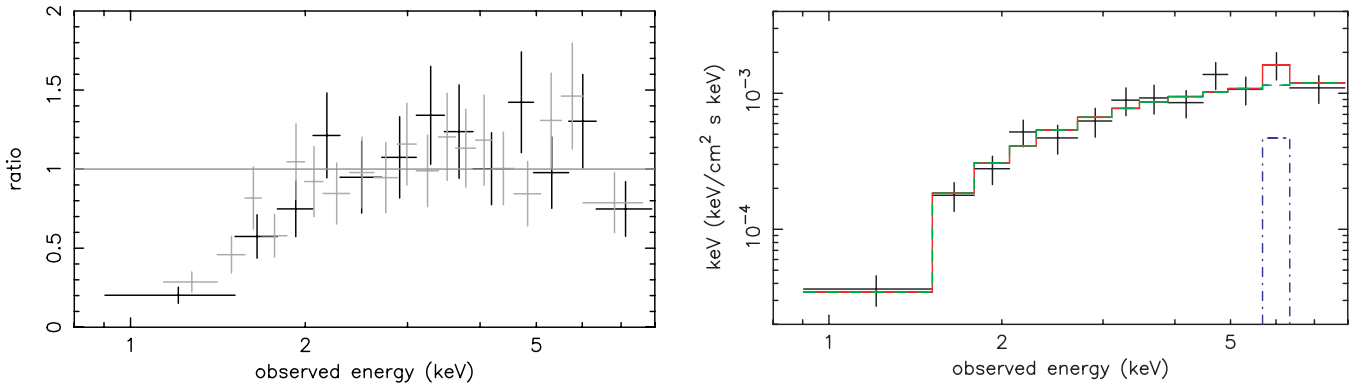

FIG. 3.—2MASS J13000534+1632149. *Left*: Ratio of pn (*black*) and MOS (*gray*) EPIC spectral data to a simple power-law fit above 2 keV, showing a strong low-energy cutoff. *Right*: Unfolded spectrum (*black*), illustrating the best-fit (*red*) attenuated power-law model (*green*). A weak Fe K emission line (*blue*) is seen near 6 keV. Only pn camera data are shown, for clarity. [*See the electronic edition of the Journal for a color version of the left panel of this figure.*]

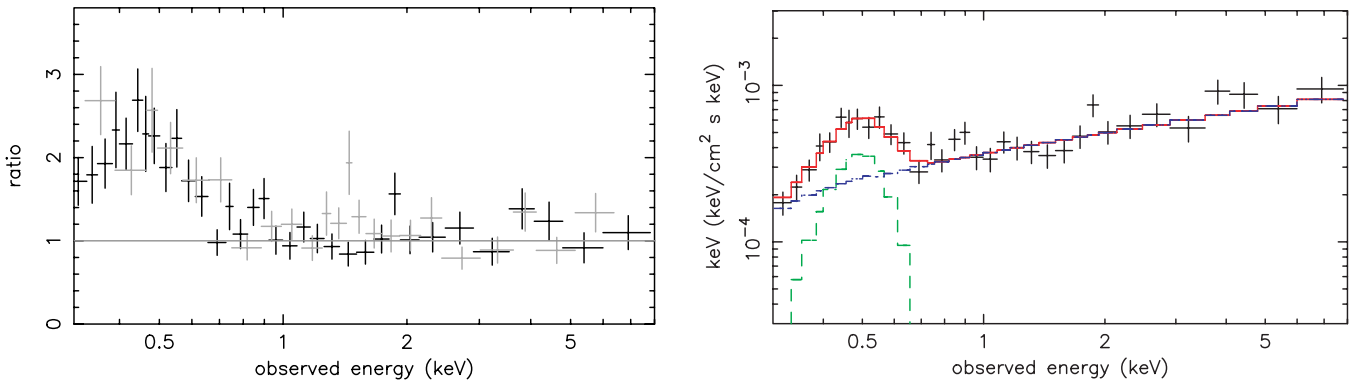

FIG. 4.—2MASS J14025120+2631175. *Left*: Ratio of pn (*black*) and MOS (*gray*) EPIC spectral data to a simple power-law fit above 2 keV, showing a soft excess when extrapolated to lower energies. *Right*: Unfolded spectrum (*black*), illustrating the best-fit model (*red*), with a power-law component (*blue*) and Gaussian soft emission component (*green*). Only pn camera data are shown, for clarity. [*See the electronic edition of the Journal for a color version of the left panel of this figure.*]

The *Chandra* observation yielded a hardness ratio HR $= -0.6$, indicating significant X-ray flux in the 0.5–2.5 keV band. The simple power-law fit (Table 2) showed a steep power law of $\Gamma = 2.0 \pm 0.4$, with no significant absorption.

Our *XMM-Newton* observation found 2MASS J14025120+2631175 to be the brightest X-ray source in the sample, at a flux level consistent with that observed by *Chandra*. A power-law fit for energies $\gtrsim$2 keV yielded moderately hard spectral indexes $\Gamma = 1.53 \pm 0.16$ (pn) and 1.4 ± 0.15 (MOS). Extrapolating this fit to 0.3 keV revealed a soft excess (Fig. 4, *left*). Modeling the soft excess with a Gaussian emission line (again, a marginally better fit than a blackbody; $\Delta\chi^2 = -4$ for -1 dof) gave an excellent fit ($\chi^2 = 110$ for 102 dof; Fig. 4, *right*). The "line" energy (AGN rest frame) was 0.44 ± 0.10 keV, with a width of $\sigma \sim 100$ eV and a flux of $\sim 4 \times 10^{-4}$ photons cm^{-2} s^{-1}. We also determine an upper limit on the X-ray column density, $N_{\rm H} \lesssim 4 \times 10^{20}$ cm^{-2} (90% confidence); including absorption at this level in the spectral fit steepens the deduced power law to $\Gamma \sim 1.6$, closer to the normal range for type 1 AGNs.

The observed fluxes (pn camera; Table 4) were 7.5×10^{-13} ergs cm^{-2} s^{-1} (0.3–1 keV), 4.7×10^{-13} ergs cm^{-2} s^{-1} (1–2 keV), and 1.9×10^{-12} ergs cm^{-2} s^{-1} (2–10 keV). The overall 0.3–10 keV luminosity was 2.6×10^{44} ergs s^{-1}, with 1.6×10^{43} ergs s^{-1} in the Gaussian soft X-ray emission component.

3.5. *2MASS J23444958+1221432*

2MASS J23444958+1221432 is classified as a type 1 QSO, lies at a redshift of $z = 0.199$, and is viewed through a Galactic column of $N_{\rm H} = 4.7 \times 10^{20}$ cm^{-2}. It has a hardness ratio HR $= -0.4$ in the *Chandra* observation, with a simple power-law fit finding a power law of $\Gamma = 2.0 \pm 0.4$, plus an absorbing column of $N_{\rm H} = (4 \pm 2) \times 10^{21}$ cm^{-2}.

Our *XMM-Newton* observation found 2MASS J23444958+1221432 to be substantially fainter than during the *Chandra* observation, by a factor of $\sim$2–3. Proceeding as before, we first fitted a power law to the data above $\sim$2 keV, obtaining typical type 1 indexes of $\Gamma = 1.70 \pm 0.16$ (pn) and 1.58 ± 0.18 (MOS). Extrapolating this fit to 0.3 keV showed the spectrum to be complex (Fig. 5, *left*), with evidence of absorption and also possibly a soft excess.

To first model the absorption, we again added `absori` to the power law, finding a reasonably good fit ($\chi^2 = 91$ for 73 dof) with a column density $N_{\rm H} = (9.7 \pm 1.5) \times 10^{21}$ cm^{-2} of moderately ionized gas. The ionization parameter $\xi = 21 \pm 9$ is constrained by the energy of the flux upturn, observed below $\sim$0.7 keV, which corresponds primarily to the absorption edge of ionized O VII in the model. However, visual examination of this spectral fit (Fig. 5, *right*) shows that the absorbed power-law model fails to match fully the observed spectral upturn.

We therefore added an emission component, modeled by a Gaussian line, obtaining a significantly improved fit of $\chi^2 = 65$ for 69 dof. As with 2MASS J09184860+2117170, this line approximates the blend of emission lines from ionized gas, and accurate modeling would require accounting for the uncertain energy calibration at $E < 0.5$ keV. In this fit the continuum curvature below $\sim$2 keV was again modeled by `absori`, while

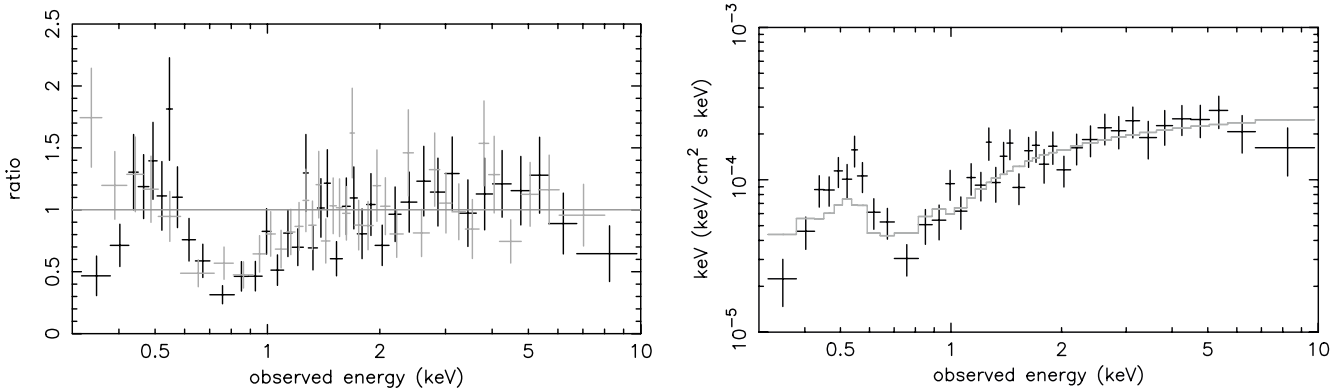

FIG. 5.—2MASS J23444958+1221432. *Left*: Ratio of pn (*black*) and MOS (*gray*) EPIC spectral data to a simple power-law fit above 2 keV, showing evidence for low-energy absorption and a possible soft excess. *Right*: Unfolded spectrum (*black*), illustrating the best-fit power-law plus photoionized absorber model (*gray*). Only pn camera data are shown, for clarity. [*See the electronic edition of the Journal for a color version of the left panel of this figure.*]

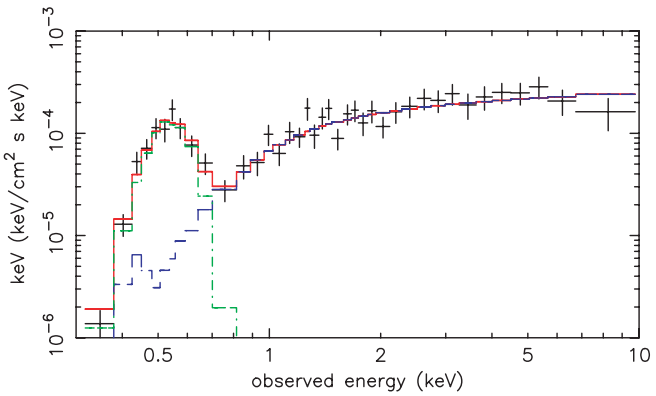

FIG. 6.—2MASS J23444958+1221432. Unfolded spectrum (*black*), illustrating the best-fit (*red*) absorbed power-law (*blue*) plus Gaussian emission component (*green*) model. Only pn camera data are shown, for clarity.

the low-energy upturn was due mainly to the Gaussian line. A consequence was that the ionization parameter of the absorbing column fell to $\xi = 0.02 \pm 0.2$. Figure 6 reproduces this "best" spectral model for 2MASS J23444958+1221432. The power-law indexes in this fit were $\Gamma = 1.86 \pm 0.12$ (pn) and 1.91 ± 0.22 (MOS). The low-ionization absorber had $N_{\rm H} = (6.5 \pm 2.6) \times 10^{21}$ cm^{-2}. The Gaussian line had an energy (AGN rest frame) of 0.64 ± 0.05 keV and a flux of 10^{-4} photons cm^{-2} s^{-1} (Table 3).

The observed fluxes derived from this best fit (pn camera; Table 4) were 9.0×10^{-14} ergs cm^{-2} s^{-1} (0.3–1 keV), 1.4×10^{-13} ergs cm^{-2} s^{-1} (1–2 keV), and 5.1×10^{-13} ergs cm^{-2} s^{-1} (2–10 keV). The overall 0.3–10 keV luminosity was 7.9×10^{43} ergs s^{-1}, with 2.9×10^{42} ergs s^{-1} in the Gaussian soft X-ray emission component.

4. DISCUSSION

The primary motivation for the *XMM-Newton* observations was to study the X-ray spectral complexity to estimate its effect on the X-ray properties of these sources in the lower S/N *Chandra* data and thus guide our assessment of the larger *Chandra* sample. Although the *XMM-Newton* exposures were typically a factor of $\sim$2 shorter than planned, due to the rejection of noisy data, the recorded counts were greater, and hence the broadband X-ray spectra were better determined than in the *Chandra* survey. For simplicity we refer to the individual AGNs using only their first four numbers; for example, 2MASS J09184860+2117170 is 2M 0918 in the following discussion. Since the spectral form is known to change with flux level in AGNs, it is important to note that 2M 1051 was brighter, while 2M 0918 and 2M 2344 were fainter, in the *XMM-Newton* observations.

4.1. *The X-Ray Properties of the 2MASS AGNs*

Our *XMM-Newton* observations showed two of our five sources to have extremely hard observed spectra ($\Gamma \lesssim 1.3$; Table 3) above 2 keV (2.16–2.37 keV, adjusted for redshift). In the case of 2M 0918, our modeling suggests that this is due to a strong (non-varying) reflection component, consistent with the low flux state during the *XMM-Newton* observation, while 2M 1300 exhibits the largest absorbing column and the only absorber with significant opacity above 2 keV. Allowing for a large reflection component in 2M 0918 and the observed cold absorption in 2M 1300 shows the underlying power-law slopes to be normal for a type 1 QSO (Table 3). These two cases show how the presence of strong reflection or a Compton-thin absorber can make the observed spectrum hard above $\sim$2 keV. In two other cases (2M 1051 and 2M 2344) the *XMM-Newton* spectra show substantial cold absorption, although not sufficient to greatly affect the spectral slope above 2 keV. For none of these four red AGNs does the intrinsic power-law continuum appear unusually hard. The fifth, 2M 1402, has a somewhat harder than average power law ($\Gamma = 1.54$) and a soft excess but no detected absorption in the *XMM-Newton* data.

A soft X-ray excess is found in all three type 1 sources (i.e., types 1–1.5: 2M 0918, 2M 1402, and 2M 2344), in each case having a luminosity of $\sim$5% of the corresponding 2–10 keV luminosity. All three soft excesses are well modeled by a Gaussian emission line centered at 0.55 ± 0.1 keV (in the AGN rest frame), providing a rough approximation to the blend of emission lines expected from ionized gas.

4.1.1. *Comparison with the Chandra Data*

The *Chandra* X-ray parameters for the five AGNs are listed, along with other multiwavelength properties, in Table 2. The *Chandra* values are generally poorly constrained. *XMM-Newton* detects complexity in three sources, two of which appeared normal in the lower S/N *Chandra* data, and variability in three. *XMM-Newton* also informs us that a simple hardness ratio is an extremely limited indicator of an AGN spectrum. In particular, using a hardness ratio to deduce the presence and amount of X-ray absorption can be highly misleading or completely wrong. Spectral hardness may be due to either absorption, as originally assumed (Wilkes et al. 2002), or a hard power-law or strong reflection component, similar to those of Seyfert 2 galaxies (Turner et al. 1997b), or hardness may be masked by a soft excess component.

The spectral parameters of the two type 2 (i.e., types 1.8–2) sources, 2M 1051 and 2M 1300, are consistent between the two observations. This is true despite the factor of 2 lower flux for 2M 1300.

The *XMM-Newton* spectrum of 2M 0918 (type 1.5) is different from that seen by *Chandra* (Tables 2 and 3). To make a direct comparison, we determined a flux-based hardness ratio ($\rm HR_F$) from the observed flux in the soft (0.3–2.5 keV) and hard (2.5–8.0 keV) bands, using the best-fit spectrum in each case. A "normal" power law ($\Gamma = 1.9$) with a typical Galactic value of $N_{\rm H}$ (3×10^{20} cm^{-2}) yields $\rm HR_F = -0.14$ using this method. For 2M 0918, the *Chandra* data give $\rm HR_F = -0.12$ (assuming no detected absorption), while for *XMM-Newton* the value is significantly harder, $\rm HR_F = 0.21$. The error on these values is $\sim$0.1 due to the uncertainty in the spectral fit. The explanation may lie in the X-ray flux being a factor of $\sim$4–5 fainter in the *XMM-Newton* observation, deduced by comparing the predicted and actual *XMM-Newton* count rates. A variable power-law component may have decreased in flux, allowing the harder (reflection dominated?) power-law continuum to dominate, while also causing the soft excess to be more visible if the latter is intrinsically less variable. The change in spectrum was confirmed by fitting the *Chandra* data with the best-fit *XMM-Newton* spectral parameters, which gave a significantly poorer fit than that listed in Table 2 ($\Delta\chi^2 = 3.4$).

The flux levels and spectral parameters for the type 1 object 2M 1402 are consistent, although *XMM-Newton* reveals a soft excess that was not visible in the *Chandra* data. The flux-based hardness ratio is harder in the *XMM-Newton* data ($\rm HR_F = -0.04$, compared with $\rm HR_F = -0.23$), suggesting some variation.

The type 1 object 2M 2344, similarly to 2M 1402, has consistent spectral parameters, but *XMM-Newton* reveals a soft excess that also masks a somewhat higher absorbing column density

than is visible in the *Chandra* data. While the *Chandra* data, with only ~250 counts, do not detect the soft excess, fitting these data with the *XMM-Newton*–deduced parameters yields a value of χ^2 similar to that for the power-law fit. Thus, despite a factor of ~2 reduction in flux in the *XMM-Newton* data, there is no evidence for spectral variability between the two observations.

Given the variety of behavior in these five AGNs, comparison of the *Chandra*-deduced $N_{\rm H}$ and flux values with those from the *XMM-Newton* data (Table 3) shows no systematic effects that could be applied to the full *Chandra* sample. While this validates any statistical results derived from the *Chandra* data, it also emphasizes that the deduced properties of individual AGNs are not reliable and that the resulting high error levels generate significant scatter.

4.2. *The Relation between X-Ray Spectral and Multiwavelength Properties*

Although this sample comprises only five AGNs, it is instructive to investigate any systematic relation between the various X-ray properties and their multiwavelength properties. Recent X-ray surveys have demonstrated that the X-ray hardness seen at fainter flux levels is generally due to absorption (Kim et al. 2004). The relation between optical-infrared colors and X-ray hardness (Mainieri et al. 2002) suggests that the obscuring material includes dust that then reddens the optical/near-IR continuum, although the dust column density is generally lower than expected on the basis of a Galactic gas-to-dust ratio (Alonso-Herrero et al. 1997; Maiolino et al. 1998). Although there are exceptions, both in individual AGNs and subsets of the population such as BAL QSOs and the red AGNs reported here, X-ray– or optically selected AGN samples show that, statistically, broad-line AGNs are soft (presumed unabsorbed) in the X-ray, while narrow-line AGNs are hard (presumed absorbed; Turner et al. 1998; Risaliti et al. 1999; Laor et al. 1997).

The two type 2 QSOs in our sample, 2M 1051 and 2M 1300, with optical types 1.9 and 2.0, respectively, are straightforward. The X-ray spectral shape is typical of AGNs, $\Gamma \sim 1.8$, and their X-ray absorption ($N_{\rm H} \sim 10^{22}$ cm^{-2}; Table 3) is at the low end of the observed range for optical type 2 AGNs (Risaliti et al. 1999). Both have significant polarized optical flux, particularly when dilution by host galaxy light is included (Table 2; Smith et al. 2003), and show broad lines in their polarized optical flux spectra. The FWHM of Hα in 2M 1300 is unusually broad, ~18,000 km s^{-1} (Schmidt et al. 2002). Interpretation as edge-on sources viewed through a significant column density of obscuring material and for which the direct nuclear light is visible due to a mirror above or below the plane of the obscuring material is standard in the unified scheme (Antonucci 1993). Any X-ray complexity is hidden in this edge-on view.

However, the three type 1 QSOs in this sample all show different behavior that does not immediately fit into a simple unification scenario. While the $B - R$ colors follow the expected trend of increased reddening as the type progresses from 1 to 2 (Table 2; B. J. Wilkes et al. 2005, in preparation), the $J - K_s$ colors appear unrelated. For example, 2M 0918, which has no detected X-ray absorption, is the reddest ($J - K_s \gtrsim 2.2$). Possibly the underlying relation between X-ray absorption and/or optical type with $J - K_s$ colors is masked by the wide intrinsic range of $J - K_s$, ± 0.5 (full range) in type 1 QSOs.

2M 1402 is a type 1 QSO with no detected X-ray absorption, normal for a type 1 source except for its unusually red $J - K_s$ color. If we assume that no absorption is present, the red color could be explained by a large amount of hot dust increasing the K_s emission.

2M 2344, also a type 1 QSO, has significant X-ray absorption. The obscuration must cover the X-ray source but not the broad emission-line region (BELR), requiring either a small, dense absorber interior to the BELR or a specific orientation with a line of sight passing through the wind above a disk or torus (Königl & Kartje 1994) that allows a view of the BELR.

2M 0918 is the most difficult to understand. It is a type 1.5 source in which the broad emission lines are partially obscured. The X-ray continuum is hard above 2 keV, but no absorption is detected ($N_{\rm H} \lesssim 1.1 \times 10^{21}$ cm^{-2}). The optical and IR continua are redder than is typical of type 1 AGNs; the former is consistent with $A_V \sim 2$ ($N_{\rm H} \sim 3.4 \times 10^{21}$ cm^{-2}, assuming a normal gas-to-dust ratio and that the Elvis et al. 1994 median spectral energy distribution is unabsorbed). This is higher than the maximum column density of cold absorbing material indicated by the *XMM-Newton* data, which is thus insufficient to explain the optical-IR continuum unless the gas-to-dust ratio is unusually low. A higher S/N *XMM-Newton* observation has been requested to check the level of X-ray absorption.

Alternatively, a significant contribution by scattered light, as in the classic case of NGC 1068 (Turner et al. 1997a), could result in the X-ray emission being dominated by the unabsorbed light from the nuclear regions, scattered off the mirror responsible for the high polarization of the optical emission. This would imply strong absorption, to suppress the direct continuum emission, and neither emission nor absorption would be detectable in the *Chandra* or *XMM-Newton* energy bands. In this case, the [O III] λ5007 line flux, which correlates strongly with the intrinsic X-ray flux in AGNs (Mulchaey et al. 1994; Turner et al. 1997a), would appear abnormally strong relative to the observed X-ray flux, and the X-ray luminosity would be unusually low. However, the $F([{\rm O\ III}])/F_{\rm X}$ ratios for the *XMM-Newton*–observed AGNs are within ~2 σ of the mean value of $\log F([{\rm O\ III}])/F_{\rm X} = -1.89 \pm 0.25$ for Seyfert 1 galaxies (Mulchaey et al. 1994); for 2M 0918 the value is -1.49 (B. J. Wilkes et al. 2005, in preparation). In comparison, the value for NGC 1068, for which the X-ray emission is known to be purely due to scattered light, the value is ~0.6. In addition, the X-ray luminosities of the AGNs in our sample are ~10^{44} ergs s^{-1}, in the normal range for AGNs (Table 3). It is thus unlikely that we are primarily observing scattered light in the X-rays.

In summary, all three type 1 QSOs can be explained by a unification model that includes lower column density material above or below the disk or torus, such as those in disk-wind models (Königl & Kartje 1994; Murray & Chiang 1995; Elvis 2000). However, additional emission and absorption from dust must also be present. Alternatives, such as a small, dense absorber, can describe individual sources, but all three cannot be described using the same scenario.

4.3. *2MASS AGNs and the CXRB*

Models of the CXRB require a significant population of X-ray–absorbed AGNs in order to match the CXRB spectrum, which is significantly flatter than that of unabsorbed AGNs (Comastri et al. 1995; Gilli et al. 2001). This population has generally been assumed to be dominated by type 2 AGNs and QSOs whose X-ray emission is generally absorbed (Turner et al. 1998). The observations have not yet found this expected population at high redshift (Bauer et al. 2004). However, the combination of X-ray hardness and visible optical broad lines in red AGNs suggests that a subset of the broad-line AGN population may also be significant contributors. The *XMM-Newton* results confirm and expand on this possibility, demonstrating that the observed

X-ray spectrum may be hard at energies above 2 keV, even where *Chandra* did *not* detect this hardness (2M 0918 and 2M 1402). All five sources are affected by absorption and/or a soft emission component at energies below ~2 keV. For 2M 0918 the *XMM-Newton* data cannot distinguish between an intrinsically hard power law and a strong reflection component that flattens the X-ray spectrum at higher energies.

Interestingly, accounting for spectral complexity in our diverse sample may explain why AGNs with apparently normal, steep continua ($\Gamma \sim 1.7$–1.9; Nandra & Pounds 1994) can more closely match the CXRB in the (observed) 2–10 keV band (Table 3). While the (unweighted) mean of the power-law indexes derived from modeling the *XMM-Newton* spectra is $\Gamma \sim 1.72$, the mean index at energies $\gtrsim$2 keV is $\Gamma \sim 1.46$ (Table 3), close to that of the integrated CXRB spectrum. This difference between observed and intrinsic spectral forms in red AGNs, which is similar to that seen in local, low-luminosity AGNs, removes the discrepancy between the spectrum of the CXRB and a subset of the AGNs that may be responsible for it.

Thus, in addition to type 2 QSOs, there are two, potentially large, subsets of the type 1 population that may contribute to the CXRB among AGNs already known from their optical/IR properties but not identified as X-ray hard in low-S/N data: those with significant X-ray absorption and those with undetected complexity. A more detailed estimation of the possible CXRB contribution of red AGNs will be reported in a separate paper (B. J. Wilkes et al. 2005, in preparation).

4.4. *Implications of the XMM-Newton Results for the Nuclear Regions of AGNs*

XMM-Newton detects a soft X-ray emission component in all three type 1 QSOs in this sample. Its form and relative luminosity, in all three cases, are similar to those found in variability studies of the bright Seyfert 1 galaxies NGC 4051 (Pounds et al. 2004a) and 1H 0419-577 (Pounds et al. 2004b), suggesting a common origin in an extended region of moderately ionized gas. Its detection in these sources with flatter high-energy slopes, where a relatively weaker power law would render a soft emission component more visible, suggests that it may be ubiquitous.

In type 1 AGNs, such as 2M 2344, strong X-ray absorption is detected by *XMM-Newton*, while the broad optical lines remain visible at the usual strength. This requires that the (cold) absorber either lies inside the BELR or is viewed at an intermediate line of sight so that the BELR remains visible. A third alternative of purely scattered broad lines is unlikely, given the normal broad emission-line strengths. If inside the BELR, such absorbing material must be of high density to survive the intense ionizing continuum. To explain the different behavior of all three type 1 QSOs in this sample with a single scenario, an intermediate viewing angle through absorbing material in a wind above or below the accretion disk or torus in current unification models (Königl & Kartje 1994; Murray & Chiang 1995; Elvis 2000) can be combined with increased hot dust emission and absorption. The two type 2 QSOs are then viewed at a more edge-on orientation so that the BELR is also obscured. The presence of a large column of cold gas, in one or more components, close to the supermassive black hole (SMBH) adds further complexity to the "unified scheme," which could help explain the classification dependence of some AGNs on the waveband being used.

5. SUMMARY

XMM-Newton observations of five red AGNs, selected as part of the 2MASS survey by their red $J - K_s$ (>2) colors, show them to have a variety of X-ray spectral forms. These results confirm and expand our earlier conclusions (Wilkes et al. 2002) that these sources are X-ray hard. Their observed emission is hard at energies above 2 keV even when it appears soft in the *Chandra* data. This hardness is due either to absorption, as is expected from a simple obscuration scenario, or to a hard (intrinsic or reflected) X-ray power law. In several sources *XMM-Newton* reveals complexity that was not apparent in the *Chandra* data, emphasizing the limitations of low-S/N data in estimating X-ray absorption and/or spectral parameters. Although the *Chandra* data can be misleading, the variety of behavior results in no systematic effects on *Chandra*-deduced parameters that could be used to guide our analysis of the larger sample.

The two type 2 sources have the simplest spectra, showing absorption of $\sim 10^{22}$ cm^{-2}, at the low end of the distribution for optical type 2 AGNs, and no further complexity. This is fully consistent with the edge-on view expected for type 2 AGNs in standard unification models. All three type 1 sources have complex spectra with a soft excess and some combination of a normal power law, reflection, and cold absorption. The soft excess is best fit by a broad Gaussian emission line, which, in this low-S/N data, provides a reasonable approximation to the blend of line emission expected from ionized gas. It may be ubiquitous, although often hard to detect due to the presence of the strong, unabsorbed, $\Gamma \sim 1.9$ intrinsic power law in most AGNs. It tends to be constant, and it may originate in an extended region of ionized gas (Pounds et al. 2005).

The mean observed X-ray spectrum of these AGNs at energies above 2 keV, $\Gamma \sim 1.46$, matches well with that of the CXRB at these energies. However, in all cases, the underlying power law has a normal, $\Gamma = 1.7$–1.9 slope (Table 3). Thus, within this red AGN sample, there is no discrepancy between the observed spectra of the AGNs and the CXRB. The combination of a hard observed X-ray spectrum above 2 keV and the presence of broad emission lines in several cases suggests two types of type 1 QSOs that have been largely overlooked as contributors to the CXRB: i.e., those with absorbed and/or complex spectra. Their contributions may be significant. Red AGNs are common at low redshift, comprising ~20% of the population that is otherwise missed in current optical surveys (Glikman et al. 2004). Their numbers at higher redshift are less well determined, since the red selection criterion is less effective at $z \gtrsim 0.6$ (Cutri et al. 2002). Improved information on their space density, in particular as a function of redshift, will soon be provided by *Spitzer-Chandra* wide-area surveys, allowing better estimates of both the importance of red AGNs to the full AGN population and their contribution to the CXRB.

Significant X-ray absorption in type 1 QSOs cannot be explained by simple unification models. To cover the X-ray source but not the broad emission-line region, the absorbing material must be either small (nuclear) or patchy. The intermediate level of the absorption, 10^{22} cm^{-2}, is suggestive of the outflowing wind or atmosphere above a disk or torus (Königl & Kartje 1994; Murray & Chiang 1995) in current unification models and thus of an intermediate viewing angle for red AGNs. This scenario can also explain the observed red optical and near-IR colors. However, it can only explain the properties of all three type 1 sources if we also invoke unusually high levels of hot dust emission and/or absorption. Thus, X-ray observations of these red AGNs will not only provide a check on the presence of absorption, but also a unique probe of the absorbing material. However, X-ray variability, which generally occurs on a much faster timescale than seen in the near-IR for radio-quiet AGNs such as these (Neugebauer & Matthews 1999), may make it hard to find a consistent picture.

The results reported here are based on observations obtained with *XMM-Newton*, an ESA science mission with instruments and contributions directly funded by ESA Member States and the USA (NASA). The authors wish to thank the SOC and SSC teams for organizing the *XMM-Newton* observations and initial data reduction. K. A. P. is pleased to acknowledge a Leverhulme Trust Emeritus Fellowship. B. J. W. and G. D. S. are grateful for the financial support of *XMM-Newton* GO grant NNG04GD27G. B. J. W. gratefully acknowledges the support of NASA contract NAS8-39073 (CXC).

REFERENCES

Alonso-Herrero, A., Ward, M. J., & Kotilainen, J. K. 1997, MNRAS, 288, 977
Antonucci, R. 1993, ARA&A, 31, 473
Arnaud, K. A. 1996, in ASP Conf. Ser. 101, Astronomical Data Analysis Software and Systems V, ed. G. H. Jacoby & J. Barnes (San Francisco: ASP), 17
Bauer, F. E., Alexander, D. M., Brandt, W. N., Schneider, D. P., Treister, E., Hornschemeier, A. E., & Garmire, G. P. 2004, AJ, 128, 2048
Comastri, A., Fiore, F., Vignali, C., Matt, G., Perola, G. C., & La Franca, F. 2001, MNRAS, 327, 781
Comastri, A., Setti, G., Zamorani, G., & Hasinger, G. 1995, A&A, 296, 1
Cutri, R. M., Nelson, B. O., Francis, P. J., & Smith, P. S. 2002, in ASP Conf. Ser. 284, AGN Surveys, ed. R. F. Green, E. Y. Khachikian, & D. B. Sanders (San Francisco: ASP), 127
Elvis, M. 2000, ApJ, 545, 63
Elvis, M., Schreier, E. J., Tonry, J., Davis, M., & Huchra, J. P. 1981, ApJ, 246, 20
Elvis, M., et al. 1994, ApJS, 95, 1
Fiore, F., et al. 2001, MNRAS, 327, 771
———. 2003, A&A, 409, 79
Francis, P. J., Nelson, B. O., & Cutri, R. M. 2004, AJ, 127, 646
Fruscione, A., & Siemiginowska, A. 2000, *Chandra* News, 7, 4
Gilli, R., Salvati, M., & Hasinger, G. 2001, A&A, 366, 407
Glikman, E., Gregg, M. D., Lacy, M., Helfand, D. J., Becker, R. H., & White, R. L. 2004, ApJ, 607, 60
Green, P. G., Aldcroft, T. L., Mathur, S., Wilkes, B. J., & Elvis, M. 2001, ApJ, 558, 109
Huchra, J., & Burg, R. 1992, ApJ, 393, 90
Kim, D., et al. 2004, ApJ, 600, 59
Kirsch, M. 2004, *XMM-Newton* Calibration Document XMM-SOC-CAL-TN-0018, http://xmm.vilspa.esa.es/docs/documents/CAL-TN-0018-2-3.pdf
Königl, A., & Kartje, J. F. 1994, ApJ, 434, 446
Laor, A., Fiore, F., Elvis, M., Wilkes, B. J., & McDowell, J. C. 1997, ApJ, 477, 93
Lehmann, I., et al. 2000, A&A, 354, 35
Magdziarz, P., & Zdziarski, A. A. 1995, MNRAS, 273, 837
Mainieri, V., Bergeron, J., Hasinger, G., Lehmann, I., Rosati, P., Schmidt, M., Szokoly, G., & Della Cecca, R. 2002, A&A, 393, 425
Maiolino, R., & Rieke, G. H. 1995, ApJ, 454, 95
Maiolino, R., Salvati, M., Bassani, L., Dadina, M., della Ceca, R., Matt, G., Risaliti, G., & Zamorani, G. 1998, A&A, 338, 781
Masci, F. J., Drinkwater, M. J., & Webster, R. L. 1999, ApJ, 510, 703
Mulchaey, J. S., Koratkar, A., Ward, M. J., Wilson, A. S., Whittle, M., Antonucci, R. R. J., Kinney, A. L., & Hurt, T. 1994, ApJ, 436, 586
Murray, N., & Chiang, J. 1995, ApJ, 454, L105
Nandra, K., & Pounds, K. A. 1994, MNRAS, 268, 405
Neugebauer, G., & Matthews, K. 1999, AJ, 118, 35
Nousek, J. A., et al. 1998, Proc. SPIE, 3444, 225
Perola, G. C., et al. 2004, A&A, 421, 491
Pounds, K. A., Reeves, J. N., King, A. R., & Page, K. L. 2004a, MNRAS, 350, 10
Pounds, K. A., Reeves, J. N., Page, K. L., & O'Brien, P. T. 2004b, ApJ, 605, 670
Pounds, K. A., Wilkes, B. J., & Page, K. L. 2005, MNRAS, 362, 784
Risaliti, G., Maiolino, R., & Salvati, M. 1999, ApJ, 522, 157
Schmidt, G. D., Smith, P. S., Foltz, C. B., & Hines, D. C. 2002, ApJ, 578, L99
Silverman, J. D., et al. 2005, ApJ, 618, 123
Smith, P. S., Schmidt, G. D., Hines, D. C., Cutri, R. M., & Nelson, B. O. 2000, ApJ, 545, L19
———. 2002, ApJ, 569, 23
Smith, P. S., Schmidt, G. D., Hines, D. C., & Foltz, C. B. 2003, ApJ, 593, 676
Soifer, B. T., et al. 1984, ApJ, 278, L71
Strüder, L., et al. 2001, A&A, 365, L18
Treister, E., et al. 2005, ApJ, 621, 104
Turner, M. J. L., et al. 2001, A&A, 365, L27
Turner, T. J., George, I. M., Nandra, K., & Mushotzky, R. F. 1997a, ApJ, 488, 164
———. 1997b, ApJS, 113, 23
———. 1998, ApJ, 493, 91
Wilkes, B. J., Schmidt, G. D., Cutri, R. M., Ghosh, H., Hines, D. C., Nelson, B., & Smith, P. S. 2002, ApJ, 564, L65
Worsley, M. A., Fabian, A. C., Barcons, X., Mateos, S., Hasinger, G., & Brunner, H. 2004, MNRAS, 352, L28